5. CONCLUSIONS

A quasi-TEM analysis of a three-line coupled microstrip structure was utilized in a search for suitable dimensions of a three-line coupler that meets certain design criteria. This facilitated the construction of design curves. Measurements performed on a prototype single-section coupler displayed good agreement with theoretical results, and practically illustrated the merit of this approach. Additionally, a wideband stepped coupler was designed with the use of conventional two-line coupler synthesis techniques. Good agreement between theoretical and measured results for the coupling was obtained. Measurements showed the coupler input ports to be well matched, and good isolation between relevant ports was achieved.

REFERENCES

1. D. Pavlidis and H. L. Hartnagel, "The Design of Three-Line Microstrip Couplers," *IEEE Trans. Microwave Theory Tech.*, Vol. MTT-24, No. 10, Oct. 1976, pp. 631–640.
2. V. K. Tripathi, "The Scattering Parameters and Directional Coupler Analysis of Characteristically Terminated Three-Line Structures in an Inhomogeneous Medium," *IEEE Trans. Microwave Theory Tech.*, Vol. MTT-29, No. 1, 1981, pp. 22–26.
3. C. Wei, R. F. Harrington, J. R. Mautz, and T. K. Sarkar, "Multiconductor Transmission Lines in Multilayered Dielectric Media," *IEEE Trans. Microwave Theory Tech.*, Vol. MTT-32, No. 4, 1984, pp. 439–450.
4. V. K. Tripathi, "On the Analysis of Symmetrical Three-Line Microstrip Circuits," *IEEE Trans. Microwave Theory Tech.*, Vol. MTT-25, No. 9, 1977, pp. 726–729.
5. W. J. Louw, "Coupled Transmission Lines Revisited," *IEEE Trans. Edu.*, Vol. E-31, No. 3, 1988, pp. 234–236.
6. J. C. Coetzee and J. A. G. Malherbe, "Analysis of a Semi Re-Entrant Microstrip Coupler," *J. Electromag. Waves Appl.*, Vol. 7, No. 4, 1993, pp. 513–531.
7. J. A. G. Malherbe, *Microwave Transmission Line Couplers*, Artech House, Norwood, MA, 1988.

Received 5-16-96

Microwave and Optical Technology Letters, 13/3, 165–169

CCC 0895-2477/96

NUMERICAL SIMULATION OF SURFACE-WAVE BAND-STOP FILTERS

Svetlana V. Boriskina
Radiophysics Department
Kharkov State University
Kharkov 310077, Ukraine

Alexander I. Nosich
Institute of Radiophysics and Electronics
National Academy of Sciences
Kharkov 310085, Ukraine

KEY TERMS

Scattering, resonators, filters, transmission and reflection coefficients

ABSTRACT

In this work the scattering of an H-polarized surface wave from a circular dielectric cylinder and a perfectly conducting infinitely thin open circular screen is analyzed by the use of the surface potential approach. Efficient numerical algorithms have been devised and applications to the band-stop filters have been discussed. Sample numerical results for the total scattered power and transmission and reflection coefficients are presented. Two types of band-stop filters are compared. © *1996 John Wiley & Sons, Inc.*

1. INTRODUCTION

Recently a number of articles related to the problem of open-waveguide mode scattering from obstacles with a resonant behavior has been published. The principle of operation of various microwave devices (such as band-stop filters) is based on the modification of the surface mode field due to these scatterers. Works [1–4] were devoted to the theoretical and experimental treatment of cylindrical dielectric resonators with whispering-gallery (WG) modes. As for the scattering of surface waves from open cavities, a circular open screen over the impedance plane and inside a dielectric slab was studied analytically in [5] and numerically in [6], and some physical features of the scattering and mode conversion were clarified.

The purpose of this study is to analyze numerically the interactions of a surface mode field with a circular cylindrical dielectric resonator and an open cavity with a circular cross section, and to discuss their applications as band-stop filters. In our treatment we took an impedance plane in the H-polarization mode as the simplest (single-mode) open waveguide. We followed at first the idea presented in [7] for scattering from a dielectric cylinder immersed into a dielectric slab waveguide. However, the procedure of reducing the integral equations to the matrix equation differs from the point-matching method developed in [7]. Taking into account the scatterer's shape, we use expansions of all functions in terms of entire-domain basis functions such as angular exponents. The remainder of the article is organized as follows.

In Section 2.1 we present the mathematical formulation of the problem of surface-wave scattering from a dielectric cylinder. First we express the scattered field in the integral form as a surface potential over the contour of the scatterer. Then, imposing the boundary conditions, we obtain the integral equations. These integral equations can be reduced to a matrix equation by using the expansion of surface potential densities and the host media Green's functions in terms of angular exponents. Resulting matrix equation can be solved numerically with the accuracy limited only by the computer's digital precision.

Section 2.2 is concerned with the scattering from a circular cavity. The main idea of the treatment is to reduce the original scattering problem to the dual series equations, and to regularize them by using the Riemann-Hilbert problem technique. This approach is based on the inversion of the static part of the full-wave operator. The resulting Fredholm second-kind matrix equation is solved numerically with guaranteed accuracy.

The formulas for the transmission and reflection coefficients and far-field radiation patterns are obtained in Section 2.3. The optical theorem, based on the conservation of energy, and the principle of reciprocity are also presented in this section. They have been employed to validate a numerical simulation.

The results of numerical analysis are depicted in Section 3. There we compare two types of resonators and discuss their advantages as applied to band-stop and rejection filters.

We conclude the article with some estimations of the method presented and suggestions for extending the analysis to more complicated problems. All field quantities are as-

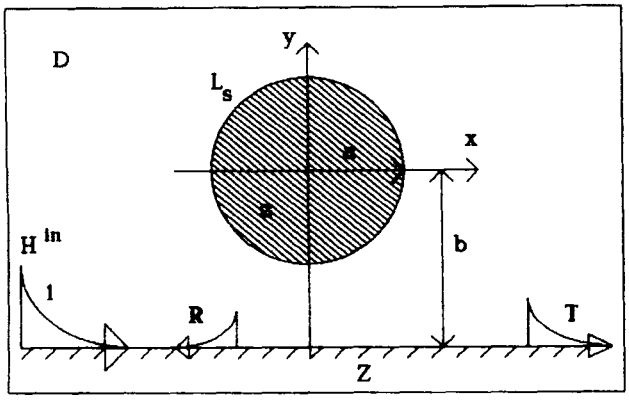

(a)

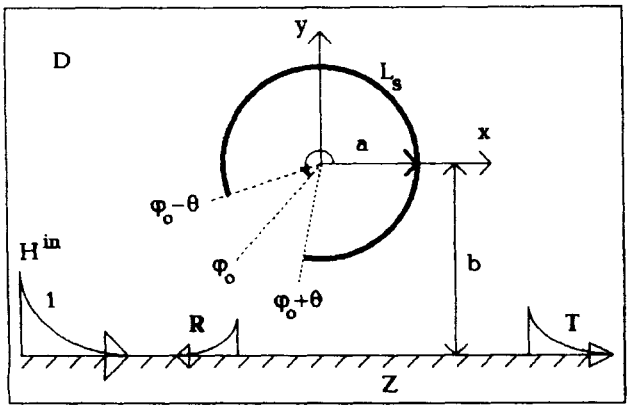

(b)

Figure 1 Geometries of the scattering problems

sumed to have time variation $\exp(-i\omega t)$, and this time factor is omitted throughout of the analysis.

2. METHOD OF ANALYSIS

2.1 Cylindrical Dielectric Resonator. Consider the scattering problem depicted in Figure 1a. An H-polarized impedance-plane surface wave is incident on the dielectric cylinder with permittivity ϵ. The total magnetic field in such a geometry consists of the incident (H^{in}) and scattered (H^{sc}) components, and

$$H^{in} = e^{-\alpha k(y+b)+ih_0kx}. \tag{1}$$

Here $\alpha = iZ$, $h_0 = \sqrt{1+\alpha^2}$, Z being the surface impedance. Note that to have the function (1) corresponding to a nondecaying surface wave, the impedance should be a purely imaginary (lossless) value. The field inside the dielectric body is denoted as H^b. The total field satisfies the Helmholtz equation:

$$(\Delta + k^2\epsilon(\vec{r}))H(\vec{r}) = 0, \qquad \vec{r} = (r,\varphi) \in D \setminus L_s, \qquad D = (x, y > -b), \tag{2}$$

boundary conditions on the contour L_s of the scatterer,

$$H^{sc} + H^{in} = H^b,$$

$$\frac{1}{\epsilon}\frac{\partial H^b}{\partial n} = \frac{\partial H^{in}}{\partial n} + \frac{\partial H^{sc}}{\partial n}, \qquad \vec{r} \in L_s, \tag{3}$$

and on the impedance plane,

$$\frac{\partial H}{\partial y} + \alpha kH = 0, \qquad y = -b, \tag{4}$$

and a modified radiation condition that takes the form

$$H^{sc}(\vec{r})\widetilde{r\to\infty}\Phi(\theta)\left(\frac{2}{i\pi kr}\right)^{1/2} e^{ikr} + \begin{Bmatrix} T-1, x>0 \\ R, x<0 \end{Bmatrix} e^{-\alpha(y+b)+ih_0|x|}. \tag{5}$$

We represent the scattered field outside and inside the dielectric resonator in terms of the single layer surface potentials:

(*) see a critical comment below

$$H^b(\vec{r}) = \int_{L_s} \varphi(\vec{r}_s)G_b(\vec{r},\vec{r}_s)\,dl_s, \tag{6}$$

$$H^{sc}(\vec{r}) = \int_{L_s} \psi(\vec{r}_s)G(\vec{r},\vec{r}_s)\,dl_s, \tag{7}$$

and obtain a pair of integral equations with respect to the unknown potential densities:

$$\int_{L_s} \varphi(\vec{r}_s)G_b(\vec{r},\vec{r}_s)\,dl_s - \int_{L_s} \psi(\vec{r}_s)G(\vec{r},\vec{r}_s)\,dl_s = H^{in}(\vec{r}), \qquad \vec{r} \in L_s \tag{8}$$

$$\frac{1}{\epsilon}\frac{\partial}{\partial n}\int_{L_s} \varphi(\vec{r}_s)G_b(\vec{r},\vec{r}_s)\,dl_s - \frac{\partial}{\partial n}\int_{L_s} \psi(\vec{r}_s)G(\vec{r},\vec{r}_s)\,dl_s = \frac{\partial}{\partial n}H^{in}(\vec{r}). \tag{9}$$

Here G_b is the Green's function of the homogeneous medium with permittivity ϵ, and G is the Green's function of the half space with a planar impedance boundary; that is,

$$G_b(\vec{r},\vec{r}_s) = \frac{i\epsilon}{4}H_0^{(1)}(k\sqrt{\epsilon}|\vec{r}-\vec{r}_s|), \tag{10}$$

$$G(\vec{r},\vec{r}_s) = \frac{i}{4}H_0^{(1)}(k|\vec{r}-\vec{r}_s|) + \frac{i}{4\pi}\int_{-\infty}^{\infty}\frac{1}{g}\cdot\frac{ig-\alpha}{ig+\alpha}e^{ikg(y+y_s+2b)+ihk(x-x_s)}\,dh, \tag{11}$$

where $g = \sqrt{1-h^2}$. Then, because of the geometry of the scatterer, these integral equations can be reduced to a matrix equation by using the expansions of potential densities and the Green's functions in terms of angular exponents:

$$\psi_m + \frac{(i)^m}{J_m(ka)(1+iB_m)} \times \sum_{n=-\infty}^{\infty}\psi_n(-1)^n(i)^nJ_n(ka)\Omega_{m+n} = -\frac{(i)^m(h_0+\alpha)^m}{J_m(ka)(1+iB_m)}e^{-\alpha kb}, \tag{12}$$

where

$$\Omega_n = -H_n^{(1)}(2kb) + \frac{2i}{\pi}\int_{-\infty}^{\infty} \frac{ig-\alpha}{ig+\alpha} e^{2ikgb}(h_0 - i\alpha)^n \, dh, \quad (13)$$

$$B_m = \frac{J_m'(k\sqrt{\epsilon}a)Y_m(ka) - \sqrt{\epsilon}J_m(k\sqrt{\epsilon}a)Y_m'(ka)}{J_m(ka)J_m'(k\sqrt{\epsilon}a) - \sqrt{\epsilon}J_m(k\sqrt{\epsilon}a)J_m'(ka)}. \quad (14)$$

The resulting matrix equation can be solved numerically to determine the coefficients of the scattered field potential density expansion. The potential density expansion coefficients of the field inside the dielectric can be obtained via the following relation:

$$\varphi_m = \frac{J_m(ka)}{\epsilon H_m^{(1)}(k\sqrt{\epsilon}a)J_m(k\sqrt{\epsilon}a)} \times \left[\psi_m H_m^{(1)}(ka) + i^m(h_0 - \alpha)^m e^{-\alpha kb} + \sum_{n=-\infty}^{\infty} \psi_n (-1)^n J_n(ka)\Omega_{m+n}\right]. \quad (15)$$

2.2 Cavity-Backed Aperture. The scattering geometry for this case is shown in Figure 1b. Let us now represent the scattered field in this geometry in the form of a double-layer potential:

$$H^{sc}(\vec{r}) = \frac{i}{4}\int_{L_s} \mu(\vec{r}_s)\frac{\partial}{\partial n_s}G(\vec{r},\vec{r}_s)\, dl_s. \quad (16)$$

As in the previous subsection, this scattered field should satisfy Eq. (2), (5), and (4), but on the cross-sectional contour of the scatterer the following relation is valid:

$$\frac{\partial H}{\partial n} = 0, \qquad \vec{r} \in L_s, \quad (17)$$

L_s being now a circular arc of the radius a. By following the procedure described in [5], we obtain the integral equation for the surface current density as

$$\frac{\partial}{\partial n}\int_{L_s}(\vec{r}_s)\frac{\partial}{\partial n_s}G(\vec{r},\vec{r}_s)\, dl_s = -\frac{\partial}{\partial n}H^{in}(\vec{r}), \qquad \vec{r} \in L_s. \quad (18)$$

Equations of this type are often encountered in scattering problems. They can be solved numerically by directly applying the method of moments. However, the solution scheme based on the analytical inversion of the static part of (18) is much more efficient. The current density function should be completed with identical zero on the slot. After expanding all the functions of (18) in terms of the angular exponents, term-by-term integrating and differentiating, we come to the dual series equations of the expansion coefficients. Furthermore, we regularize them by inverting the static part analytically [5] and arrive at the following Fredholm second kind of matrix equation:

$$\mu_m = \sum_{n=-\infty}^{\infty}\left[\Delta_n T_{mn} + i\pi(ka)^2(-1)^n i^n J_n'(ka) \times \sum_{p=-\infty}^{\infty} i^p J_p'(ka)\Omega_{p+n}T_{mp}\right]\mu_n + i\pi(ka)^2\sum_{n=-\infty}^{\infty} T_{mn}i^n J_n'(ka)(h_0 - i\alpha)^n e^{-\alpha kb}, \quad m = 0, \pm 1, \ldots, \quad (19)$$

where the coefficients T_{mn} are the functions of φ_0 and θ and can be found in [5, 6]. They are easily computed as combinations of exponents and the Legendre polynomials.

2.3 Far-Field Characteristics and Procedure Validation. To obtain the amplitudes of the guided mode at $x \to \pm\infty$ along the interface, one has to use the contour deformation in the complex h plane and take account of the residues at the poles $h = \pm h_0$:

$$\begin{Bmatrix} T-1 \\ R \end{Bmatrix} = \frac{4\alpha}{h_0}e^{-\alpha kb}\sum_{(n)}\xi_n(\mp i)^n S_n(h_0 \pm \alpha)^n. \quad (20)$$

The far-field scattering patterns can be evaluated by applying the steepest-descent method to the integrals in (7) and (16) in the far zone of the scatterers:

$$\Phi(\varphi) = \sum_{n=-\infty}^{\infty}\xi_n(-i)^n S_n \times \left(e^{in\varphi} + \frac{i\sin\varphi - \alpha}{i\sin\varphi + \alpha}e^{2ikb\sin\varphi - in\varphi}\right). \quad (21)$$

Here ξ_n denotes φ_n for the dielectric resonator or μ_n for the cavity, and S_n is $J_n(ka)$ or $J_n'(ka)$, respectively.

The optical theorem, based on the energy conservation principle, serves as an independent partial check of the numerical codes. In addition, the theorem can be used to minimize the time needed to compute the total radiated power, as

$$P_{sc} \equiv \frac{4\alpha}{\pi h_0}\int_0^{\pi}|\Phi(\varphi)|^2\, d\varphi = 1 - |T|^2 - |R|^2. \quad (22)$$

For the case of the cavity scatterer, the reciprocity theorem should also be satisfied:

$$T(\varphi_0) = T(\pi - \varphi_0). \quad (23)$$

This means that the transmission coefficient of the incident mode is invariant of the direction of incidence.

For three-digit accuracy in practical computations, it is enough to take the matrix truncation numbers as $N_{diel} = ka\sqrt{\epsilon} + 3$ and $N_{cav} = ka + 10$, respectively. As for the optical theorem and the reciprocity, they were satisfied with a 10^{-13} accuracy for all the values of the problem parameters. CPU time varies depending on the size of the scatterers. For example, computing a dielectric cylinder of $ka = 2$, $\epsilon = 10$, with the PC AT-486, 40 MHz and MS-DOS Fortran took 8 s. For a cavity of $ka = 2$ it took 7 s.

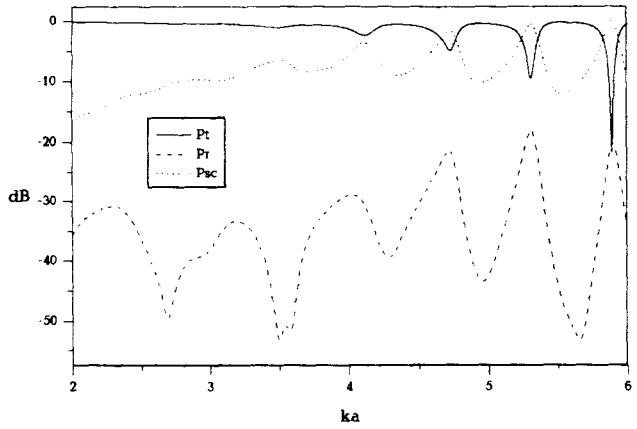

Figure 2 Far-field scattering characteristics versus ka for the dielectric resonator ($\epsilon = 4$, $b/a = 1.1$, $h_0 = 1.5$)

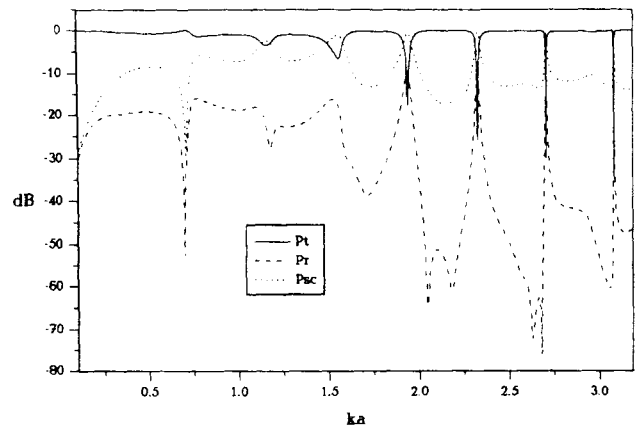

Figure 3 Far-field scattering characteristics versus ka for the dielectric resonator ($\epsilon = 10$, $b/a = 1.5$, $h_0 = 1.5$)

3. NUMERICAL RESULTS AND DISCUSSION

Let us first consider the dielectric resonator. In Figures 2 and 3, the plots of the far-field characteristics are shown as a function of the normalized frequency parameter ka. One can see that a dielectric cylinder can be used as a band-stop filter. The principle of operation of such a filter is based on the excitation of a WG mode in the resonator. At the resonances the filter characteristics were calculated versus the spacing. The results are plotted in Figure 4. In order to obtain an optimum performance, the spacing between the plane and the resonator must be selected properly.

The dielectric cylinders show the advantages of WG-mode resonators, such as high quality factor and periodicity of stop bands. Because of these advantages, the filters on WG-mode resonators have undergone considerable development and are widely used in various microwave active and passive components. Note that the transmission level gets lower with the increasing the resonant frequency. Besides, in order to work on a high-Q resonance one must either enlarge the cylinder radius or use dielectrics with large permittivity. However, the latter may lead to considerable ohmic losses. It is worth noting that our accurate analysis shows that at High-Q WG resonances the incident mode power may be 99% converted to the radiation field.

Using an open metal cavity is a way to avoid these difficulties and minimize the electric size of the filter. A high-Q-

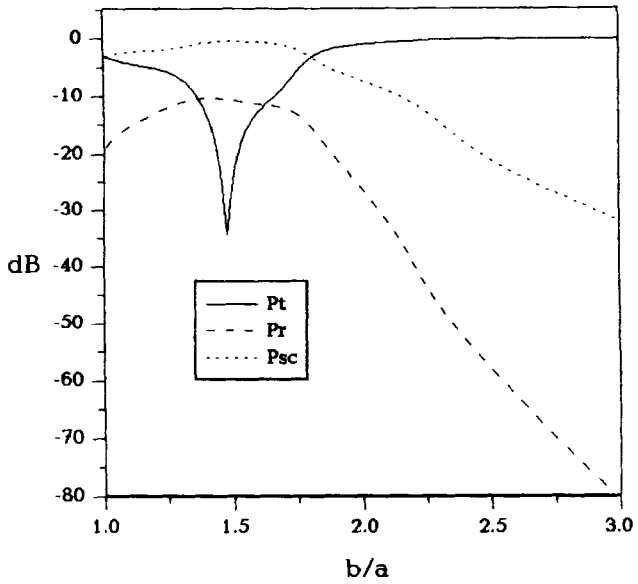

Figure 4 Far field scattering characteristics versus the spacing between the dielectric resonator and the impedance plane ($\epsilon = 10$, $ka = 2.707$, $h_0 = 1.5$)

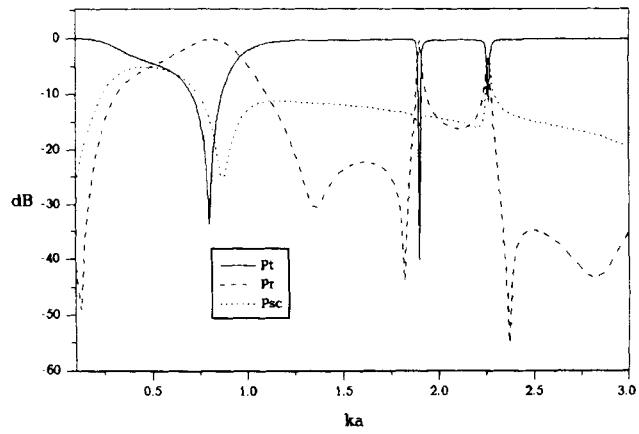

Figure 5 Frequency dependences of the far-field characteristics for scattering from the cavity ($b/a = 1.5$, $\theta = 30°$, $\varphi = 270°$, $h_0 = 1.5$)

value resonance with a lower level of radiation losses can be observed when the radius of the cylinder is smaller than the wavelength. Figures 5 and 6 show the typical frequency dependences of transmitted ($P_T = |T|^2$), reflected ($P_R = |R|^2$), and scattered (P_{sc}) power fractions for the scattering from the metal slotted cavity. When excited by the surface-mode field, the cavity gives a resonant response provided that the incident-wave frequency coincides with the real part of a complex eigenmode frequency. Because of the splitting of the closed cylinder's doubly degenerated modes, these eigenfunction can be related to two families of modes, symmetric and antisymmetric ones, by cutting a slot. It can be observed that antisymmetric resonances have a larger Q factor then symmetric ones. The first low-frequency peak is due to the Helmholtz mode of a cavity-backed aperture (see [5, 6]). The Helmholtz-mode frequency is a complex number tending to zero when $\theta \to 0$. So, by narrowing the slot one can obtain a miniature low-frequency rejection filter with a remarkably low parasitic radiation: More than 90% of the incident mode power may be converted to the reflected mode.

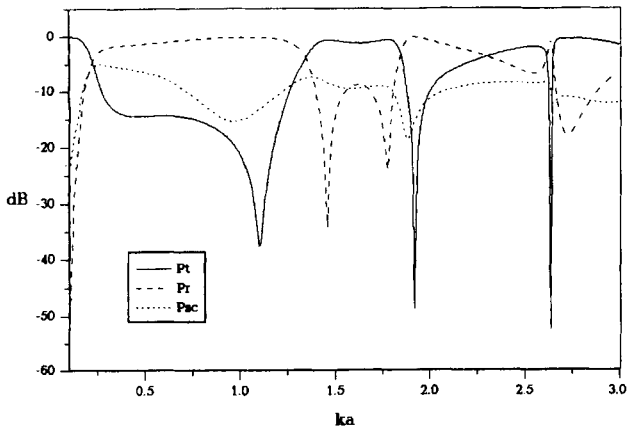

Figure 6 Frequency dependences of the far-field characteristics for the same geometry as in Figure 5 but $b/a = 1$

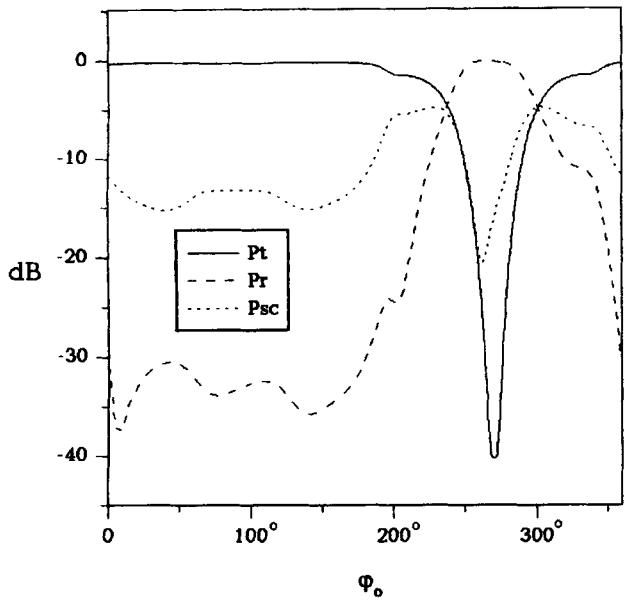

Figure 7 Effect of the cavity's rotation on the far-field scattering characteristics ($ka = 1.898$, $b/a = 1.5$, $\theta = 30°$, $h_0 = 1.5$)

The values of transmission and reflection coefficients depend considerably on the cavity orientation. So, unlike the dielectric resonators, coupling with the waveguide can be varied by rotating the cavity. The plots in Figure 7 demonstrate the effect of the cavity's rotation on the far-field characteristics.

4. CONCLUSIONS

The proposed method is well suited to the analysis of band-stop filters. Based on this approach, efficient numerical techniques were developed, and rejection, transmission, and radiated-field characteristics were calculated. Implementation of the approach is considered here only for H-mode scattering, but this method can also solve the discontinuity problems with an E-mode incidence.

Sharp resonant phenomena were observed for scattering from dielectric cylinders and metal cavities. These effects can be used for the design of band-stop filters in surface-wave guides. Our investigations proved the advantages offered by such resonators, and these advantages led to excellent performances of microwave oscillators and filters. Although the presented numerical examples deal the impedance-plane surface-wave scattering from obstacles, the method is applicable to various types of incident fields (plane wave, dielectric slab eigenmode, etc.), and different host media.

We emphasize that due to the regularization, our solutions are equally accurate near the sharp resonances, unlike the conventional method-of-moments ones (see [8]). BEcause of this, the former can be used for the computer-aided design of resonant microwave devices.

ACKNOWLEDGMENTS

The authors would like to express their thanks to Dr. A. G. Yarovoy for many helpful discussions. Also, the support of SUMMA Foundation is acknowledged with gratitude.

REFERENCES

1. N. Morita, "Scattering and Mode Conversion of Guided Modes of a Slab Waveguide by a Circular Cylinder," *IEE Proc. Pt. H*, Vol. 27, No. 5, 1980, pp. 263–169.
2. X. H. Jiao, P. Guillon, L. A. Bermudez, and P. Auxemery, "Whispering-Gallery Modes of Dielectric Structures: Applications to Millimeter-Wave Bandstop Filters," *IEEE Trans. Microwave Theory Tech.*, Vol. MTT-35, No. 12, 1987, pp. 1169–1175.
3. V. I. Kalinichev and P. N. Vadov, "A Numerical Investigation of the Excitation of a Dielectric Resonator," *Sov. J. Commun. Technol. Electron.* (English Transl.), Vol. 33, No. 7, 1988, pp. 108–115.
4. Y. Filipov, S. Kharkovsky, A. Kirichenko, "WG Modes of Nonuniform Dielectric Resonators," *Microwave Opt. Technol. Lett.*, Vol. 10, No. 2, Oct. 1995, pp. 124–129.
5. A. I. Nosich, "Scattering of the Surface Wave of an Open Impedance Waveguide by an Unclosed Cylindrical Screen," *Soviet Phys. Tech. Phys.* (Engl. Transl.), Vol. 31, No. 8, 1986, pp. 883–889.
6. A. I. Nosich and A. S. Andrenko "Scattering and Mode Conversion by a Screen-Like Inhomogeneity inside a Dielectric Slab Waveguide," *IEEE Trans. Microwave Theory Tech.*, Vol. MTT-42, No. 2, 1994, pp. 298–307.
7. A. G. Yarovoy, "Surface Potential Method in the Wave Scattering from Localized Inhomogeneities of a Planar Dielectric Waveguide," *IEICE Trans. Electron. (Jpn.)*, Vol. E78-C, No. 10, 1995, pp. 1440–1446.
8. G. L. Hower, R. G. Olsen, J. D. Earls, and J. B. Schneider, "Inaccuracies in Numerical Calculations of Scattering near Natural Frequencies of Penetrable Objects," *IEEE Trans. Antennas Propagat.*, Vol. AP-41, No. 7, 1993, pp. 982–986.

Received 5-20-96

Microwave and Optical Technology Letters, 13/3, 169–173

CCC 0895-2477/96

(*) The field representation in terms of only the single-layer potential (6).(7) is not the most general one and leads to the appearance of the spurious (real-valued) eigenvalues of resulting IE. They spoil the algorithm because the IE condition number has poles at the spurious-eigenvalue frequencies. The severity of assocoated numerical error depends, however, on the details of the IE discretization scheme used. The full remedy is the use of the Muller IE which is completely equivalent to the original boundary-value problem and thus free of spurious eigenvalues.

ANALYSIS OF A DUAL PERIODIC STRIP GRATING

D. Saji Stephen, Thomaskutty Mathew, C. K. Aanandan, P. Mohanan, K. A. Jose, and K. G. Nair
Department of Electronics
Cochin University of Science and Technology
Cochin 682022, India

KEY TERMS

Blazing, electromagnetic waves, reflection, scattering, strip grating